

Optically detected magnetic resonance of the bismuth-on-metal-site intrinsic defect in photorefractive sillenite crystals

H.-J. Reyher, U. Hellwig, and O. Thiemann

Universität Osnabrück, FB Physik, Postfach 4469, D-4500 Osnabrück, Federal Republic of Germany

(Received 29 June 1992; revised manuscript received 20 October 1992)

Applying the method of optically detected magnetic resonance (ODMR) via the magnetic circular dichroism (MCD) of absorption, paramagnetic resonance data are provided for the ground state of the intrinsic defect Bi_M in sillenites of the type $\text{Bi}_{12}\text{MO}_{20}$ ($M = \text{Si}, \text{Ge}, \text{Ti}$). This is a characterization on a microscopic scale of this defect, generally being present at very high densities in these crystals, which are very interesting for photorefractive applications. The g values are slightly larger than g_{free} and the hyperfine constants A , accounting for the interaction with the central bismuth nucleus, are of the order of 19 GHz [g/A for $\text{Bi}_{12}\text{SiO}_{20}$:2.049(5)/19.35(6) GHz; $\text{Bi}_{12}\text{GeO}_{20}$:2.041(3)/19.21(5) GHz; $\text{Bi}_{12}\text{TiO}_{20}$:2.05(1)/19.2(1) GHz]. Both parameters were found to be isotropic within the experimental error. The theoretical interpretation of g and A leads to the picture of a highly covalent defect, which consists of a hole mainly located on the oxygen neighbors of the tetrahedrally coordinated Bi_M^{3+} ion. The MCD spectra of the sillenite crystals are linked to the ODMR results by the method of tagged MCD and are thus identified to arise from this defect. Since MCD is related to absorption, this identification provides evidence for the attribution of the broad 2.6-eV absorption band, specific to sillenites, to Bi_M .

I. INTRODUCTION

Crystals of sillenite structure such as $\text{Bi}_{12}\text{MO}_{20}$, where M stands for Si, Ge, or Ti, have attracted great interest, because they are promising materials for applications based on the photorefractive effect.¹ By this effect one means the creation of a refractive index pattern by imposing a light intensity distribution on the crystal. There is general agreement that the basic mechanism for the generation of the photorefractive index change consists in a charge transfer process caused by the illumination. The charge carriers, electrons, or holes are produced by photoionization of deep traps, move over certain distances by diffusion, by drift in an electric field, or by the photovoltaic effect, and finally become trapped again by the same or by other types of deep defects in the material. Space charge fields grow up, which finally induce changes of the refractive index by the Pockels effect.

From the above it becomes clear that defects play a decisive role in photorefractive materials. Their characterization on a microscopic level may give important information for the understanding of the photorefractive "performance" or even for the development of novel properties of the crystals.

In the case of $\text{Bi}_{12}\text{MO}_{20}$ -type sillenites, it has been stated,² that nearly all the crystals used in experiments concerning the photorefractive properties were grown from nominally undoped material. Therefore, one is led to assume that an intrinsic defect is at least partially responsible for the photorefractive effect in $\text{Bi}_{12}\text{MO}_{20}$ crystals.³ As a candidate, one can find in the literature the Bi_M defect ($M = \text{Si}, \text{Ge}, \text{Ti}$), which was proposed to be present in $\text{Bi}_{12}\text{MO}_{20}$ at densities up to 10^{20} cm^{-3} .^{4,5}

There are arguments,⁴ that this abundant intrinsic defect is responsible for the typical amberlike hue of the crystals. This color is connected with a broad, unstructured absorption band reaching from the band edge ($\approx 3.2 \text{ eV}$) up to about 2.2 eV. Other authors proposed a "Si vacancy complex" to be the cause of this absorption band in $\text{Bi}_{12}\text{SiO}_{20}$.⁶ In a recent paper⁷ it has been stated that there is no direct experimental evidence for any of these two models and that iron should play the most important role in the photoinduced processes in sillenites.

Figure 1 outlines the unit cell of $\text{Bi}_{12}\text{MO}_{20}$ (space group $I23$) showing the geometrically perfect⁸ oxygen tetrahedra around each M ion. Each MO_4 complex is surrounded by sevenfold oxygen coordinated bismuth ions, which are not shown for the sake of clarity. The Bi_M defect is thought to consist of a Bi ion instead of M in one of the oxygen tetrahedra.

Since optical absorption represents the first step in the photorefractive process, it is desirable to identify unambiguously by microscopic methods the defects which are responsible for the observed absorption bands. One way to do this is to perform EPR measurements and to correlate the EPR signals with the optical absorption bands. This has been done for a number of extrinsic impurities in sillenites, such as Fe, Mn, Cr, etc.⁹⁻¹² In these publications, the authors report among other things a strong increase of the broad absorption band at 2.6 eV, when the crystals are illuminated by light above or near the band edge. The growth of the absorption is accompanied by either a decrease or an increase of the EPR signals of the transition elements. This correlation between EPR and absorption reflects a charge transfer between the transition elements and either an intrinsic defect or

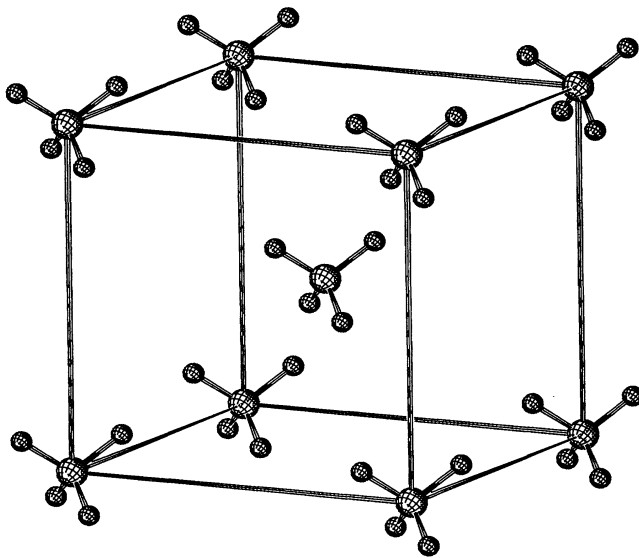


FIG. 1. Unit cell of $\text{Bi}_{12}\text{MO}_{20}$ with space group $I23$. The low symmetry Bi-O complexes are omitted and only the MO_4 tetrahedra are shown here. The defect under consideration is formed simply by replacing M by Bi in one of the tetrahedra.

iron, which is always present in sillenites as unintentional doping. The broad-band absorption may therefore be attributed to either an unknown intrinsic defect or to Fe^{2+} . The latter conclusion has been drawn in Ref. 11, because the authors observed the increase of the 2.6-eV band to be correlated with a decrease of the EPR of Fe^{3+} in their sample. On the other hand, there exist crystals for which the photoinduced growth of absorption at 2.6 eV is connected with a slight increase of the EPR amplitude of Fe^{3+} .¹⁰ Hence, the attribution of the 2.6-eV absorption band to Fe^{2+} (Ref. 11) seems to be doubtful. In contrast, the results shown below provide evidence that this band is related to the Bi_M defect. As mentioned in the previous paragraph, this finding also agrees with results obtained with quite different methods.^{4,5}

In this paper we shall report on the observation of paramagnetic resonance of the Bi_M defect in sillenites. The EPR signals have been detected by the optically detected magnetic resonance (ODMR) method via the magnetic circular dichroism (MCD) of absorption. In the next section it will be shown that the method of ODMR via MCD is able to connect EPR signals with information on the optical absorption in a rather direct way. One may say that the MCD bands are tagged by the EPR "fingerprint."¹³ This is a more compelling method than the often used procedure of measuring EPR and absorption spectra one by one and then looking for changes in both spectra due to light exposure or heat treatment of the crystals.

The direct correlation of absorptive and paramagnetic properties by tagged MCD is a most interesting task in view of the gain of information about the photorefractive effect. In this paper, however, the ODMR data of the

Bi_M defect in sillenites and their interpretation are the main topic. The reasons for this are the following: (i) The range of the spectra of "MCD tagged by ODMR" of the Bi_M center has not yet been extended to wavelengths below 450 nm and a complete comparison with the absorption data cannot be made until now. (ii) The only way to obtain structural information on Bi_M is by ODMR, no EPR of this defect being known in $\text{Bi}_{12}\text{MO}_{20}$. This is because of the fact that for the more commonly used EPR frequencies (9–35 GHz) no transition is possible with the usually accessible magnetic fields (see below). Also, experiments at 3 GHz have been unsuccessful, probably because of sensitivity problems. Information on the paramagnetic properties of Bi^{4+} is rather scarce in literature: There exists a work concerning the EPR of the radical BiF_6^{2-} (Ref. 14) and a paper reporting on cross-relaxation signals from Bi^{4+} with F centers in KCl, detected by MCD.¹⁵ Unfortunately, no EPR parameters are given in Ref. 15, but we know from private communication that there seem to exist several types of Bi centers in KCl with parameters similar to those observed for Bi_M in $\text{Bi}_{12}\text{MO}_{20}$.

II. EXPERIMENT AND METHOD

The properties of the samples are listed in Table I. All specimens had a size of approximately $3 \times 2.5 \times 2 \text{ mm}^3$. The edge of 2 mm was mounted parallel to the optical axis of the setup and was either a [100] or a [110] direction. Most measurements were done using [110] samples.

The method of ODMR via the MCD of absorption has been described in Ref. 13 (in this review ODMR is called ODESR and MCD of absorption is abbreviated by MCDA). Therefore, only a brief description of the applied technique will be given here: The light from a xenon arc lamp passes through a monochromator and enters a photoelastic modulator, which switches between right and left circularly polarized light at a rate of 40 kHz. The modulated beam is focused onto the crystal, which is mounted in a LHe cryostat in the center of a superconducting Helmholtz magnet (longitudinal field B up to 3 T). The transmitted light intensity is detected by a photomultiplier or a silicon diode. The ac and dc parts of the detector current, I_{ac} and I_{dc} , are recorded and form the MCD signal, as will be explained in the next paragraph. Irradiating the crystal by microwaves at resonance field B_{res} will cause paramagnetic transitions to occur between the magnetic sublevels of the ground state of the center under investigation. These EPR transitions show up in the MCD signal, also to be discussed below. For the sillenites we used X -, Q -, and W -band frequencies.

TABLE I. Sample data.

Crystal	Doping	Source
$\text{Bi}_{12}\text{SiO}_{20}$	nominally undoped	France
$\text{Bi}_{12}\text{GeO}_{20}$	nominally undoped	USSR
$\text{Bi}_{12}\text{TiO}_{20}$	(a) nominally undoped (b) 1000 ppm Mn	Dr. Hesse, University of Osnabrück

As a basis for further discussion, we briefly want to mention some fundamental MCD formulas: One possibility to define the MCD is¹⁶

$$\text{MCD} = \ln(e) d (\alpha_l - \alpha_r),$$

where α_l and α_r are the absorption coefficients for left and right circularly polarized light and d is the thickness of the crystal. With the usually valid assumption $d(\alpha_l - \alpha_r) \ll 1$, it follows from the expansion of the exponential function in the Lambert-Beer law that $\text{MCD} \propto I_{\text{ac}}/I_{\text{dc}}$.

It is well known from Stephens' classical work¹⁷ that the MCD can be separated into two diamagnetic terms (A and B terms) and a paramagnetic one (MCD_p or C term), which dominates for broad absorption bands, particularly at the low temperatures of typically 2 K, which are used in our setup. So we have $\text{MCD} \approx \text{MCD}_p \propto (\alpha_l - \alpha_r)$. Using a number of usually well justified approximations, Stephens has shown that the MCD_p for one band can be expressed by a rather simple formula

$$\begin{aligned} \text{MCD}_p \propto f(E)E \sum_{mi} G_{mi}(B, T) \\ \times \sum_{mf} \left[|\langle i, mi | r^- | f, mf \rangle|^2 \right. \\ \left. - |\langle i, mi | r^+ | f, mf \rangle|^2 \right]. \end{aligned}$$

$G_{mi}(B, T)$ represents the (thermal) occupation probability of a magnetic sublevel of the initial or ground state $|i, mi\rangle$; the matrix elements are those of the electric dipole operators r^- or r^+ for left or right circularly polarized light between the initial and the final states $|f, mf\rangle$. Finally, $f(E)$ stands for the shape function of the absorption band belonging to the $i \rightarrow f$ transition, in dependence of the energy E of the light. If several final states f and hence several bands $f(E)$ are present, the respective terms are simply summed up to form the total MCD_p . For a paramagnetic ground state, one can always group the n sublevels (i, mi) into pairs of time conjugate states $\pm|mi\rangle$, plus a single level if n is odd. Because of time reversal symmetry one has

$$\sum_{mf} \left[|\langle i, -|mi\rangle | r^- | f, mf \rangle|^2 - |\langle i, -|mi\rangle | r^+ | f, mf \rangle|^2 \right] = - \sum_{mf} \left[|\langle i, +|mi\rangle | r^- | f, mf \rangle|^2 - |\langle i, +|mi\rangle | r^+ | f, mf \rangle|^2 \right].$$

Hence, the above relation describing MCD_p can be rewritten as

$$\begin{aligned} \text{MCD}_p \propto f(E)E \left[\sum_{|mi|} [G_{-|mi|}(B, T) - G_{+|mi|}(B, T)] \sum_{mf} \left[|\langle i, |mi\rangle | r^- | f, mf \rangle|^2 - |\langle i, |mi\rangle | r^+ | f, mf \rangle|^2 \right] \right. \\ \left. + \text{a term for } mi = 0 \text{ for odd } n \right]. \end{aligned} \quad (1)$$

With the exception of a possible state $|mi = 0\rangle$, the MCD_p consists of a sum (over $|mi|$) of terms which are proportional to the polarization of the time conjugate pair states $|\pm|mi|\rangle$. At low temperatures the polarization factors $P_{|mi|} = G_{-|mi|}(B, T) - G_{+|mi|}(B, T)$ and thus the MCD_p will generally increase if the magnetic field grows from zero. An equivalent equation is derived in Ref. 17 for a Kramers doublet as state $|i\rangle$. It has been put in a more general form here, because the present paper deals with a more complicated ground state.

Equation (1) shows that the following types of spectra can be measured: (i) To obtain a *MCD spectrum* one records $\text{MCD}_p(E)$, keeping B at a fixed value. The field should be high enough to achieve substantial values for the individual $P_{|mi|}$. Such a spectrum is proportional to $f(E)$, the shape function of the absorption band for the $i \rightarrow f$ transition. In general this fact connects the MCD with the absorption spectra. The possible exception is given by the case that the difference of the matrix elements in (1) is zero. This leads to a so called MCD-silent band. (ii) To record an *ODMR spectrum*, E is kept constant and B is swept through a resonance value, with microwave power incident on the crystal. Paramagnetic transitions between the states $|i, mi\rangle$ will drive the P_{mi}

away from the thermal equilibrium values and a change of the MCD intensity will arise. (iii) The last type of spectrum, *MCD tagged by ODMR* or simply tagged MCD (TMCD), is measured by switching the microwave power on and off while B is at the resonance value for a specific paramagnetic transition. This procedure yields the amplitude of the ODMR signal, which is now recorded in the desired range of E to provide the TMCD spectrum. The main difference between TMCD and MCD spectra consists in the selectivity of the former one: In the often encountered case that optical bands from several centers are overlapping, a TMCD spectrum will filter out the contribution of the "EPR-active" center to the total MCD. In this way MCD and hence absorption spectra can be correlated with EPR or, more precisely, with ODMR transitions.

III. EXPERIMENTAL RESULTS

A. MCD and TMCD

The dots in Fig. 2 show the MCD spectrum of $\text{Bi}_{12}\text{TiO}_{20}:\text{Mn}$ for photon energies between about 1.5 eV (the cutoff of our detection system) and approximately

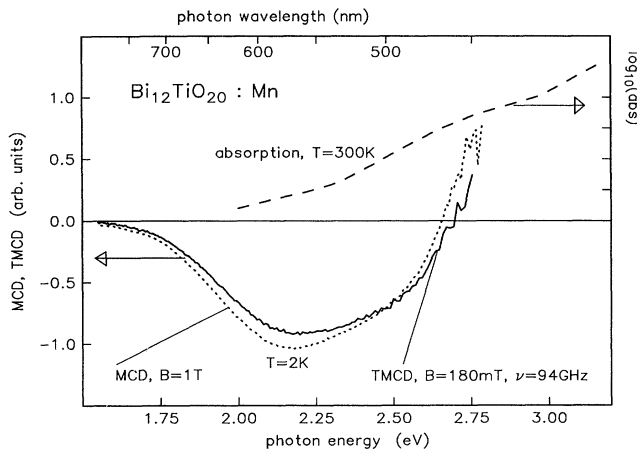


FIG. 2. MCD (dotted line) and TMCD (solid line) spectra of $\text{Bi}_{12}\text{TiO}_{20}:\text{Mn}$. Both spectra have been brought to the same scale. For comparison the dashed line shows a typical absorption spectrum of $\text{Bi}_{12}\text{TiO}_{20}$ (logarithmic scale).

2.75 eV. Above 2.75 eV the intensity of the transmitted light was too low because of the strong increase of the absorption approaching the band gap. In the future, this limit will be extended to higher values using thinner crystals ($d \leq 0.5$ mm). The spectrum in Fig. 2 has been recorded at relatively low light intensities in order to avoid otherwise observed changes of the MCD amplitude caused by illumination with photon energies higher than 2.2 eV. This effect has not yet been examined in detail, but it seems to be connected with the photosensitivity of the MCD of sillenites reported in Ref. 18.

The structure of the MCD bands was found to be very similar for all crystals listed in Table I and also agrees very well with that found by other authors¹⁸ in nominally undoped $\text{Bi}_{12}\text{GeO}_{20}$. From this we conclude that the MCD spectrum depicted in Fig. 2 is a common feature for all $\text{Bi}_{12}\text{MeO}_{20}$ type crystals and is related to an intrinsic defect rather than to extrinsic impurities. In Fig. 2, especially, there is no evidence for a contribution of Mn ions to the MCD, although the spectra depicted there have been measured with a Mn-doped crystal and the conventional EPR of Mn (Ref. 10) has been identified in this sample. Manganese is expected to show a rather characteristic absorption band at 1.7 eV in sillenites.¹⁰

A typical absorption spectrum of sillenite crystals is shown by the dashed line in Fig. 2, where the ordinate represents the logarithm of the absorbance. One is tempted to relate the broad band at 2.6 eV to the observed MCD. This was first suggested in Ref. 18, because the MCD crosses the zero line in the vicinity of the maximum of this absorption band, a behavior which has also been observed for the V^- center in MgO .¹⁹ Indeed, many basic defects such as e.g., F centers in alkali halides²⁰ or the As_{Ga} antisite in GaAs (Ref. 21) show derivativelike MCD bands at the position of an absorption band. These MCD bands of type “pseudo-A” (Ref. 17) are composed of two C-term bands, each described by Eq. (1), with opposite signs resulting from the relative size of the dipole

matrix elements in Eq. (1). Since there are MCD bands around 2.6 eV, it is obvious that Bi_M shows absorption there. But as long as there exists no quantitative theoretical description of both absorption and MCD bands of $\text{Bi}_{12}\text{MO}_{20}$, it is not justified to attribute the broad absorption at 2.6 eV totally to the Bi defect. The experience taken from MCD studies of other defects, such as, e.g., the V^- center, can yield only plausible arguments for such an identification.

Observing the MCD shown in Fig. 2 at an arbitrarily chosen value of E , ODMR signals of Bi_M could be detected, which will be presented and analyzed in the next section. In order to identify the MCD spectrum by this ODMR, we measured the the TMCD spectrum, i.e., the amplitude of one of the ODMR transitions (to be shown below) versus the photon energy (solid line in Fig. 2). Apart from a small shift of the zero crossing, which might be due to a zero field offset in the spectrum represented by the dotted line in Fig. 2, the TMCD is identical with the MCD spectrum. That means that one can unambiguously state now that the broad MCD bands in $\text{Bi}_{12}\text{MO}_{20}$ crystals result from the intrinsic defect Bi_M .

In conclusion, the MCD bands in the region 1.5–2.75 eV are linked to the Bi_M center by ODMR. Therefore, according to Eq. (1), the absorption bands $f(E)$ in that region are, at least partially, due to this defect. Keeping in mind that the assignment given in Ref. 4 of the 2.6-eV absorption band to Bi_M is based on experimental findings, which are not related to MCD and ODMR investigations, our results confirm this attribution in an independent way.

B. ODMR

Figure 3 shows the change of the MCD caused by cw microwave transitions in the ground state of the Bi_M

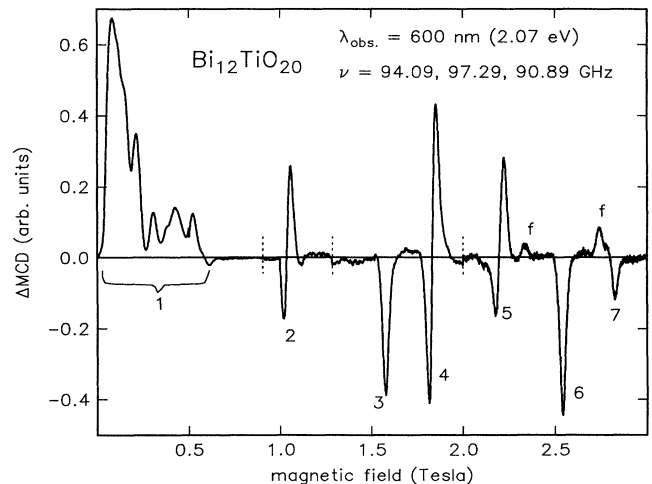


FIG. 3. ODMR at W-band frequencies (cw excitation) of $\text{Bi}_{12}\text{TiO}_{20}$. A smooth base line corresponding to the MCD in thermal equilibrium is subtracted after recording. The amplitudes of the signals in various parts of the spectrum differ appreciably and have been scaled to appear in approximately the same size. The numbers indicate allowed transitions; f marks forbidden ones.

defect. A smooth base line corresponding to the thermal equilibrium values for the polarization factors $P_{|mi|}$ in Eq. (1) has been subtracted after recording and the signals above 1 T have been magnified to appear in approximately the same size as the giant low field transitions marked by 1. The hump in this region consists of a number of unresolved resonance lines. The resolved lines, such as, e.g., No. 3, possess a relatively large linewidth [full width at half maximum (FWHM) ≈ 36 mT]. This ODMR spectrum was recorded with the monochromator set to 600 nm (2.07 eV), near the maximum of the MCD spectrum. The microwave source (impatt diode) operated at 94.09 GHz with strong sidebands at ± 3.2 GHz. A positive signal in Fig. 3 indicates a polarization enhancement of the ground-state sublevels relative to the Boltzmann equilibrium. This feature will be explained below by relaxation effects for the derivativelike resonances 2, 4, and 5. These effects are furthermore responsible for a very slow growth and decay of the ODMR signals. When the microwave is switched on and off with B at the resonance value for, e.g., signal 3, it takes about 2 min at $T=2$ K for a complete buildup and decay of this signal. In order to get a quick overview the scan times were chosen to be shorter than it would be necessary to have adiabatic conditions. It was checked that by this compromise an uncertainty of about ± 10 mT results for the positions of the resonances. The same applies for the resonances which could be observed for the frequency ranges 34.5–35.7 and 8–11 GHz.

The ODMR signals from crystals with (100) and (110) surfaces were at the same positions within this systematic error of ± 10 mT. All plausible kinds of defect axes would show different positions of resonances for these two orientations, if substantial anisotropy was present. In view of this, we used an isotropic Hamiltonian to analyze the ODMR spectra:

$$H = g\beta\mathbf{BS} - g_n\beta_n\mathbf{BI} + \mathbf{AIS}. \quad (2)$$

The first two terms represent the electronic and the nuclear Zeeman effect, respectively, and the third term accounts for the hyperfine interaction. All transitions for W -, Q -, and X -band frequencies can be explained by this Hamiltonian for $S=1/2$ and $I=9/2$, the nuclear spin of ^{209}Bi (100% natural abundance, $g_n\beta_n = 7.14$ MHz/T). The eigenvalues of (2) are described by the Breit-Rabi formula (e.g., Ref. 22) and are plotted in Fig. 4 for values of g and A suitable to our problem. We use the quantum numbers (F, M_F) of the total angular momentum operator as labels of the levels throughout the whole range of the magnetic field.

The transitions corresponding to the resonances in

TABLE II. Parameters g and A for Bi_M in sillenites.

Crystal	g	A / GHz
$\text{Bi}_{12}\text{SiO}_{20}$	2.049 (5)	19.35 (6)
$\text{Bi}_{12}\text{GeO}_{20}$	2.041 (3)	19.21 (5)
$\text{Bi}_{12}\text{TiO}_{20}$	2.05 (1)	19.2 (1)

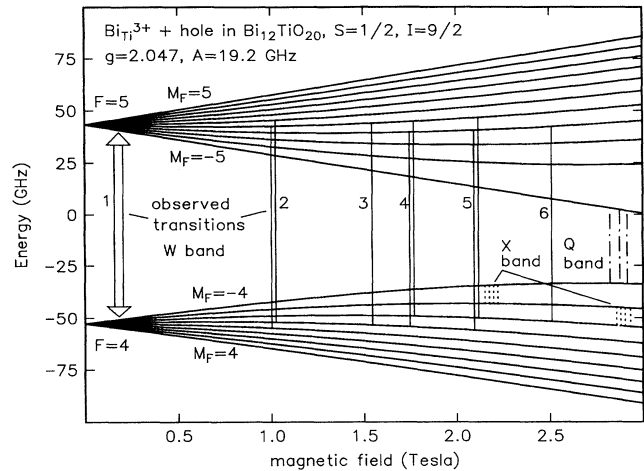


FIG. 4. Breit-Rabi diagram for a system $S=1/2$, $I=9/2$, appropriate to Bi^{3+} + hole in sillenites. The numbers of the transitions correspond to those in Fig. 3. Line 7 as well as those marked by f in Fig. 3 are omitted here for the sake of clarity [$7 \equiv (F=4, M_F=-2) \leftrightarrow (5, -2)$ for 97.296 GHz, $f \equiv (4, -3/-1) \leftrightarrow (5, -1/-3)$ for 90.89 and 94.089 GHz].

Fig. 3 are marked, as well as those observed with various Q - and X -band frequencies. Certain well resolved resonances in the W band and all lines in the Q and X bands have been taken into account to find the appropriate parameters g and A . Only the results of the measurements with [110]-cut samples were taken into account here.

In the case of $\text{Bi}_{12}\text{GeO}_{20}$ and $\text{Bi}_{12}\text{SiO}_{20}$ the transitions observed for all the three frequency ranges could be explained simultaneously by the above Hamiltonian using the parameters given in Table II. The errors in Table II result from the experimental error of ± 10 mT for the position of the resonance lines. For both crystals the measurements with X -band frequencies yielded a slightly larger g value in comparison to that obtained from Q - and W -band results, but this deviation was not significant with respect to the experimental errors. The same deviation was also observed for $\text{Bi}_{12}\text{TiO}_{20}$. In this case, however, the experimental uncertainty could not explain the discrepancy. Therefore, for this crystal the error intervals of g and A in Table II have been chosen in such a way as to allow a simultaneous description of the transitions observed in all frequency ranges by Eq. (2). The differences just mentioned may be due to the existence of a nuclear electric quadrupole effect, to be discussed below.

IV. DISCUSSION

In this section we will discuss (i) the EPR parameters δg and A , (ii) the possible influence of nuclear quadrupole interaction on the spectra, and (iii) the origin of derivativelike ODMR signals depicted in Fig. 3.

(i) Interpretation of the values of A and δg : The large values of the hyperfine constant listed above as well as the observed multiplicities for electronic spin $S = 1/2$

and nuclear spin $I = 9/2$ indicate that the electron (or hole; see below) of the defect is at least partially located on a Bi ion. The predominantly isotropic EPR spectra suggest the local symmetry to be cubic. Hence, the most plausible defect model is Bi_M^{4+} with one unpaired $6s$ electron, which is tetrahedrally coordinated by oxygen atoms. Among the more abundant isotopes with $I=9/2$ only ^{93}Nb and ^{115}In might be acceptable candidates for omnipresent residual impurities responsible for the observed ODMR signals instead of Bi_M . But in the charge states appropriate to the host crystals considered here both ions have paramagnetic configurations due to d electrons. The large observed values for A therefore exclude this possibility.

In view of the chemical instability of Bi^{4+} , it was proposed^{4,5} to regard the Bi_M defect in $\text{Bi}_{12}\text{MO}_{20}$ as a Bi^{3+} ion associated with a hole h , i.e., $\text{Bi}^{3+}+h$. This point of view is confirmed by a comparison of A of the defect with that of free Bi, for which we found a value of $A_{\text{free}} = 77$ GHz from Hartree-Fock atomic wave functions including a relativistic correction.²³ The relatively large value of A_{free} results from the $6s$ wave function of bismuth. We therefore find a reduction for A of approximately 75%, if Bi is on a M site in $\text{Bi}_{12}\text{MO}_{20}$. Such a decrease of A is usually interpreted²⁴ as to result from a covalent delocalization of the charge carrier onto the atomic orbitals of the ligands, the oxygen atoms in our case. Only a probability of 25% is left for the hole to reside in the Bi $6s$ state. In conclusion, the A values of Bi_M in $\text{Bi}_{12}\text{MO}_{20}$ fully justify the nomenclature $\text{Bi}_M^{3+}+h$, which emphasizes the strongly covalent character of the defect.

In addition, the observed positive g shift supports this point of view: Iida²⁴ has calculated the g shift δg for ns^1 ions, which are tetrahedrally coordinated by group-VI ions having a $(n's)^2(n'p)^6$ configuration, the adequate situation for our problem. Hole delocalization is taken into account by hybridizing the $A_1(6s)$ central wave function with the corresponding ligand states. By the spin-orbit interaction $(n'p\pi)$ ligand states of T_1 symmetry are admixed to the totally symmetric A_1 ground state. This admixture causes the g shift, and the following formula is derived [negligible²⁴ terms in Iida's formula (2.8) are omitted here]:

$$\delta g = \frac{4\sqrt{2}}{3}\gamma_1\gamma_2N\lambda_\sigma. \quad (3)$$

Here, γ_1 stands for the coefficient of the $|a_1\rangle$ part in the low energy eigenstate, which diagonalizes the spin-orbit operator, and γ_2 for the $|t_1\pi\rangle$ part therein. N is the normalization constant of $|a_1\rangle$ and λ_σ the fraction of the $(n'p\sigma)$ admixture to this state. Although not mentioned by Iida, the following equality can easily be shown [by calculating the eigenvectors of (2.4) from Ref. 24]:

$$\gamma_1 = -\frac{1}{\sqrt{2}}\gamma_2N\lambda_\sigma\frac{\zeta_p}{E}, \quad (4)$$

ζ_p being the spin-orbit interaction constant, which has been defined to be positive in Ref. 24, since the spin-orbit

Hamiltonian for hole states is written there as $-\zeta_p I_s$. As the eigenvalue E of the spin-orbit matrix turns out to be negative for the ground state [see (2.5) in Ref. 24], we finally obtain from (3) and (4) that δg is positive, as observed.

It has been shown for defects with s character²⁵ that the positive contribution to the g shift, discussed above, may be overcompensated by a negative one, which again results from admixtures to the ground state of the defect caused by the spin-orbit coupling. Yet, in this case, mixing occurs with conduction-band-like states. This negative δg outweighs the positive term, if the defect level is closer to the conduction than to the valence band. Hence, the Bi_M defect should lie close to the valence band. Again, this finding agrees well with Refs. 4 and 5, where the onset at about 2.2 eV of the broad 2.6-eV absorption band in $\text{Bi}_{12}\text{GeO}_{20}$ and $\text{Bi}_{12}\text{SiO}_{20}$ has been taken as the energy distance between the ground state of the defect and the conduction band [band gap ≈ 3.2 eV at room temperature (RT)].

(ii) Hints at the influence of the nuclear quadrupole effect on the spectra: It has been stated above that there is a certain discrepancy between the results for X -band measurements on one hand and those at Q - and W -band frequencies on the other. Since we could not find any systematic experimental error causing this problem, we will discuss now whether the inclusion of nuclear electric quadrupole interaction in the spin Hamiltonian can resolve the problem.

Electric nuclear quadrupole interaction requires a quadrupole moment of both the nucleus, which is known to exist for ^{209}Bi , and the electronic wave function, which does *not* exist for a state of A_1 symmetry. From physical arguments it seems to be likely that the Bi_MO_4 cluster is distorted to some extent and that the actual symmetry is lower than tetrahedral. Additional incorporation of Bi ions instead of Ge, Si, or Ti in the core of the crystal boules causes an appreciable increase of the lattice constant there.⁴ Consequently, since there is a considerable mismatch between the ionic radii of Bi^{4+} and the regular ions (see Fig. 5 in Ref. 4), one may expect a local distortion of the tetrahedra, possibly yielding axial symmetry. The hole may reside preferentially on one of the Bi-O bonds, leading to an axial center with $[111]$ direction. In this case, anisotropic g and A values would result. It is true that this was not observed, but it might be possible that the resulting anisotropy is small in comparison with the experimental error while, at the same time, the quadrupole effect is observable. We therefore tentatively added a quadrupole term $H_q = P[I_z^2 - \frac{1}{3}I(I+1)]$ to the Hamiltonian (2). This form of H_q may be obtained as an approximation for negligible anisotropy of g and A [see Eq. (3.62) in Ref. 26]. Indeed, including H_q with $P \approx -3$ MHz a more consistent description of both X -band and Q - and W -band results is found. On the other hand, positive values of P increase the discrepancy.

However, the parameter P contains the direction cosine of the defect axis with respect to the direction of the magnetic field. Consequently, for the used configuration centers with both signs of P should exist and the quadrupole term should lead rather to a broadening than

to a shift of the resonance lines. An explanation for the observation of just one sign of P might be the following: The optical transitions underlying the ODMR signal may select centers, which possess a certain orientation with respect to the optical axis, the latter being equivalent to the direction of the magnetic field in our setup. In other words, it may be possible, that the ODMR “sees” mainly those defect centers with an orientation resulting in a negative P . This speculation will be checked by doing complete sets of ODMR measurements at all three microwave bands with differently cut samples.

As a further hint at the existence of the quadrupole interaction, we want to discuss the derivativelike transitions (e.g., No. 4 in Fig. 3). These transitions are of the type $(F = 4, M_F) \leftrightarrow (F = 5, M_F - 1)$ at the low field position with a negative sign and at the high field position of type $(F = 4, M_F - 1) \leftrightarrow (F = 5, M_F)$ with a positive one. The origin of the difference in signs will be explained below. A fit with two oppositely directed Gaussians leads to linewidths, which are comparable to those of isolated transitions (e.g., No. 3 in Fig. 3). Therefore, despite the problem of long relaxation times, these fits should yield a good estimate for the separation of the strongly overlapping signals. By this procedure, the distance between the line positions was found to be about 20 mT. In contrast, a separation of about 4 mT is calculated with the Breit-Rabi formula, caused by the nuclear Zeeman interaction. Including again the nuclear quadrupole term H_q with $P \approx -3$ MHz, a line separation of the experimentally observed order of magnitude results. Positive values for P are leading to closer distances between the two transitions, or even to an interchange of the resonance positions. Therefore, the line structure for the $\Delta M_F = 1$ transitions should either be more complicated than it is assumed in the fit or centers of distinct orientations leading to negative P are “filtered out” by the ODMR method, as discussed above.

Finally, forbidden transitions are observed with a change of the projection of the total angular momentum $\Delta M_F = 2$ (lines marked by f in Fig. 3). Such transitions are “induced” by off-diagonal terms omitted in H_q .²⁶

(iii) Derivativelike ODMR signals: The derivativelike structure of the transitions just mentioned can be explained with the help of Fig. 5, where a part of the level diagram is shown. The microwave transitions are indicated by solid lines, the allowed relaxation paths between the $F = 5$ and the $F = 4$ system ($\Delta F = 1$) by dashed lines, and those within the M_F levels of either one of these systems ($\Delta F = 0$) again by solid ones. Because of the increasing phonon spectral density, it is plausible that the relaxation transitions with $\Delta F = 1$ (≈ 100 GHz) should be much faster than those with $\Delta F = 0$ (≈ 10 GHz). Assuming this to be true, it becomes clear from Fig. 5, even without setting up rate equations, that the transitions shown on the left part will lead to a decrease of the polarization of the $F = 4$ sublevels, while the paths on the right will result in an increase. Therefore, the resonance to the left will decrease the MCD signal resulting from the Boltzmann equilibrium [thermal values for the $P_{|m_i|}$ defined below Eq. (1)], whereas the one to the right will enhance it. Furthermore, since at resonance the equi-

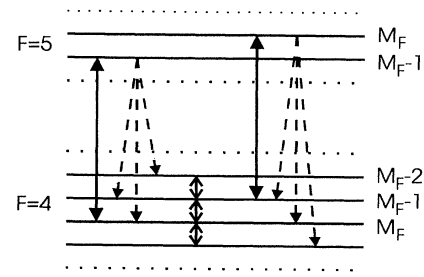


FIG. 5. Part of the Breit-Rabi diagram of Fig. 4 for constant B depicting the mechanism of “microwave pumping” (see text). One of the close pairs of microwave transitions (e.g., No. 5 in Fig. 3) is represented by solid lines. Fast allowed relaxation transitions are indicated by dashed lines; the slow relaxation paths between neighboring levels are marked by the small double arrows.

librium population of the M_F sublevels is built up via the slow relaxation paths with $\Delta F = 0$, it becomes clear now why the resonance signal grows up so slowly if the microwave is switched on. The last point clearly applies to all kind of microwave transitions, because in any case the rate at which the new equilibrium is attained is limited by the slow relaxation paths with $\Delta F = 0$.

V. CONCLUSIONS

The presumably most important intrinsic defect in sillenites, such as $\text{Bi}_{12}\text{SiO}_{20}$, $\text{Bi}_{12}\text{GeO}_{20}$, or $\text{Bi}_{12}\text{TiO}_{20}$, has been identified by ODMR to consist of a Bi^{3+} ion associated with a hole. The hole is mainly localized on the oxygen neighbors. This strongly covalent character of the defect has been revealed by the analysis of both the g value and the hyperfine constant observed for this center. Since the ODMR spectra show no anisotropy within the experimental error, the defect is situated in an essentially cubic environment. Hence, $\text{Bi}^{3+} + h$ resides on a Si, Ge, or Ti site having tetrahedral local symmetry. All the above statements fully support earlier assumptions^{4,5} based on crystallographic and optical absorption measurements. Furthermore, our “tagged MCD” measurements show that the strong paramagnetic MCD of sillenite crystals¹⁸ is due to $\text{Bi}_M^{3+} + h$. In agreement with Ref. 18, we postulate that the observed MCD spectrum is related to the very broad absorption band at about 2.6 eV, commonly found in sillenites. Consequently, this band must at least partially be attributed to the Bi defect, a finding which is also consistent with Refs. 4 and 5.

To prove definitely the existence of the nuclear quadrupole effect in the ODMR spectra is a very interesting task for future work. It would be one of the rare cases where this effect shows up in paramagnetic resonance.

ACKNOWLEDGMENTS

We thank Professor O.F. Schirmer for many helpful discussions and critical remarks and Dr. H. Hesse and

his group for supplying us with very fine crystals. We are also indebted to Dr. A. Hofstaetter, University of Giessen, for lending us the 94-GHz equipment. The support of the Deutsche Forschungsgemeinschaft, Grant No. SFB 225/C4, is gratefully acknowledged.

-
- ¹ *Photorefractive Materials and Their Applications I*, edited by P. Günter and J.P. Huignard, Topics in Applied Physics Vol. 61 (Springer-Verlag, Berlin, 1988).
- ² F.P. Strohkendl and R.W. Hellwarth, *J. Appl. Phys.* **62**, 2450 (1987).
- ³ M. Tapiero, J.G. Gies, N. Benjelloun, J.C. Launay, and J.P. Zielinger (unpublished).
- ⁴ R. Oberschmid, *Phys. Status. Solidi A* **89**, 263 (1985).
- ⁵ B.C. Grabmaier and R. Oberschmid, *Phys. Stat. Solidi A* **96**, 199 (1986).
- ⁶ S.L. Hou, R.B. Lauer, and R.E. Aldrich, *J. Appl. Phys.* **44**, 2652 (1973).
- ⁷ I. Földvári, L.E. Halliburton, G.J. Edwards, and L. Ötsi, *Solid State Commun.* **77**, 181 (1991).
- ⁸ S.C. Abrahams, P.B. Jamieson, and J.L. Bernstein, *J. Chem. Phys.* **47**, 4034 (1967).
- ⁹ H.J. von Bardeleben, *J. Phys. D* **16**, 29 (1983).
- ¹⁰ W. Wardzyński, H. Szymczak, M.T. Borowiec, K. Pataj, T. Łukasiewicz, and J. Żmija, *J. Phys. Chem. Solids* **46**, 1117 (1985).
- ¹¹ M.G. Jani and L.E. Halliburton, *J. Appl. Phys.* **64**, 2022 (1988).
- ¹² W. Wardzyński, H. Szymczak, K. Pataj, T. Łukasiewicz, and J. Żmija, *J. Phys. Chem. Solids* **43**, 767 (1982).
- ¹³ J.-M. Spaeth and F. Lohse, *J. Phys. Chem. Solids* **51**, 861 (1990).
- ¹⁴ A.R. Boate, J.R. Morton, and K.F. Preston, *J. Chem. Phys.* **67**, 4302 (1977).
- ¹⁵ P.G. Baranov and N.G. Romanov, *Appl. Magn. Res.* **2**, 361 (1991).
- ¹⁶ S.B. Piepho and P.N. Schatz, *Group Theory in Spectroscopy* (Wiley, New York, 1983).
- ¹⁷ P.J. Stephens, in *Advances in Chemical Physics*, edited by I. Prigogine and Stuart A. Rice (Wiley, New York, 1976), Vol. 35.
- ¹⁸ B. Briat, C. Laulan, J.C. Launay, and J. Badoz (unpublished); B. Briat, C. Laulan Boudy, and J.C. Launay, *Ferroelectrics* **125**, 467 (1992).
- ¹⁹ E.H. Izen, R.M. Mazo, and J.C. Kemp, *J. Phys. Chem. Solids* **34**, 1431 (1973).
- ²⁰ *Physics of Color Centers*, edited by W.B. Fowler (Academic, New York, 1968).
- ²¹ B.K. Meyer, J.-M. Spaeth, and M. Scheffler, *Phys. Rev. Lett.* **52**, 851 (1984).
- ²² M. Tinkham, *Group Theory and Quantum Mechanics* (McGraw-Hill, London, 1964).
- ²³ J.R. Morton and K.F. Preston, *J. Magn. Reson.* **30**, 577 (1978).
- ²⁴ T. Iida, *J. Phys. Chem. Solids* **33**, 1423 (1972).
- ²⁵ O.F. Schirmer and M. Scheffler, *J. Phys. C* **15**, L645 (1982).
- ²⁶ A. Abragam and B. Bleaney, *Electron Paramagnetic Resonance of Transition Ions* (Clarendon, Oxford, 1970).